A Wide-Band Self-Complementary Tightly-Coupled Dipole Array With ±80° Scanning Range in the E Plane

CHANGHAI HU[ID], **BING-ZHONG WANG**[ID], (Senior Member, IEEE),
BIN FENG SUN[ID], **REN WANG**[ID], (Member, IEEE),
SHAOQIU XIAO[ID], (Member, IEEE),
SAN-QIANG TONG[ID], (Graduate Student Member, IEEE),
AND XIAO DING[ID], (Member, IEEE)

Institute of Applied Physics, University of Electronic Science and Technology of China, Chengdu 610054, China

Corresponding author: Bing-Zhong Wang (bzwang@uestc.edu.cn)

ABSTRACT When a magnetic current antenna is parallel to a metal ground, it can produce a nearly 180° 3dB beamwidth in the E plane, which can achieve a wide-angle scanning range in the E plane. But the bandwidth of an equivalent magnetic current antenna is usually narrow. Therefore, we propose a self-complementary tightly-coupled dipole array (SC-TCDA) to achieve a wide-band magnetic current antenna, which has a wide-angle scanning range. A reflective cavity is added below the SC-TCDA. And a wide-angle impedance matching (WAIM) layer is added on the SC-TCDA. For an infinite array, the SC-TCDA can work over the band of 1.85-6.05 GHz (VSWRs<2.5) at the broadside, scan to ±80° in the E plane over the band of 2.2-5.95 GHz (VSWRs<2.5), ±40° in the H plane over the band of 1.9-6 GHz (VSWRs<2.5), and ±70° in the D plane over the band of 1.85-6.15 GHz (VSWRs<2.5). The efficiencies in different planes are greater than 80% for an infinite array. The profile of the proposed SC-TCDA is only 0.14 wavelengths at 2.2 GHz. An SC-TCDA with 16 × 16 elements is fabricated and measured. The measured and simulated results are in good agreement.

INDEX TERMS Wide-band magnetic current antenna, tightly coupled dipole array, self-complementary, wide-angle impedance matching.

I. INTRODUCTION

There is a great demand for phased arrays at present in the military and civilian areas, especially for the wide-band and wide-angle scanning phased arrays. If the phased arrays want to scan to a large angle, the antenna elements need a wide 3dB beamwidth. An ideal magnetic current above a perfect electrical conductor (PEC) plane can achieve a 180°-wide uniform radiation pattern in the E plane [1]. In [2], a microstrip magnetic dipole Yagi array antenna was proposed, which realized endfire radiation and vertical polarization over the band of 4.85-5.5 GHz. In Ref. [3], a patch magnetic current antenna was proposed, which can achieve a 180° 3dB beamwidth over

a narrow band, and the phased array achieved a scan range of ±77° over the band of 5.73-5.97 GHz. Although the above equivalent magnetic current antenna can realize wide-angle scanning in the E plane, the bandwidth is relatively narrow. Another antenna that can be equivalent to magnetic current antenna is the slot antenna [4], [5]. The slot region can be replaced by a magnetic current above a PEC ground plane [4]. In Ref. [6], a slot array with an ideal feeding network was used to achieve a wide-band and wide-angle scanning. And the calculated results show that the slot array can achieve a bandwidth of 40% when scanning to 70° in the E plane. In Ref. [7], a dielectric lens was loaded above the connected slot array antenna, which achieved a 3:1 bandwidth and about ±30° scanning range. In Ref. [8], artificial dielectric superstrates were loaded above the slot array, which achieved a

The associate editor coordinating the review of this manuscript and approving it for publication was Bilal Khawaja[ID].

2.2:1 bandwidth and a 50° scanning in all azimuth planes, but the number of the artificial dielectric superstrate layers reached 13 layers. In Ref. [9], the slot array with artificial dielectric superstrates achieved ±50° scanning in all azimuth planes with a 5:1 bandwidth, but the number of the artificial dielectric superstrate layers reached 11 layers.

Here, a self-complementary tightly-coupled dipole array (SC-TCDA) is proposed, which can scan to ±80° in the E plane. Usually, the bandwidth of a TCDA is increased by using capacitive coupling between the dipole antennas [10]–[12]. The self-complementary antenna element of the TCDA can be equivalent to the slot antenna loaded with an inductor [6]. Then, a wide 3dB beamwidth can be obtained in the E plane, which is very advantageous for large angle scanning. Although the 3dB beamwidth of the antenna element is very wide, the impedance matching of the array will become seriously bad when it scans to a large angle. Therefore, a WAIM layer is needed to be loaded over the antenna to achieve a good impedance matching [8], [9], [13]. Finally, an SC-TCDA with one dielectric layer is proposed. For an infinite array, the proposed SC-TCDA can work over a band of 1.85-6.05 GHz with VSWRs less than 2.5 at the broadside, scan to ±80° in the E plane with VSWRs less than 2.5 over the band of 2.2-5.95 GHz, ±40° in the H plane with VSWRs less than 2.5 over the band of 1.9-6 GHz, and ±70° in the D plane with VSWRs less than 2.5 over the band of 1.85-6.15 GHz. The efficiencies in different planes are greater than 80% for an infinite array. The profile of the proposed SC-TCDA is only 0.14 wavelengths at 2.2 GHz. At last, an SC-TCDA with 16 × 16 elements is fabricated and measured. The measured and simulated results are in good agreement. Section II provides the analysis and design of the SC-TCDA. Section III shows the simulated and measured results. Finally, a brief conclusion is drawn in Section IV.

II. SELF-COMPLEMENTARY TCDA
A. ANTENNA STRUCTURE
The proposed SC-TCDA is shown in Fig. 1. The parts marked with gray color are the perfect metal conductors. The parts marked with light blue color are the dielectric substrates. The parts marked with red color are the discrete ports. In order to analyze the SC-TCDA, a 4 × 4 TCDA without the feeding network and the WAIM layer is shown in Fig. 1(a). The coupling capacitances at the end of dipoles in Fig. 1(a) are interdigital capacitances, which can increase the bandwidth [10]–[12]. Fig. 1(b) is the self-complementary of Fig. 1(a) [14], which is without the feeding network and the WAIM layer. The array in Fig. 1(b) can be equivalent to the slot antennas loaded with inductors [6]. But in Fig. 1(b), the polarization of the array is changed. The direction of electric field in Fig. 1(a) is horizontal, but the direction of the electric field in Fig. 1(b) is vertical.

According to the theoretical model and simulation results in [6], the slot array has wide-band and wide-angle characteristics. However, the theoretical model is without the feeding network. The scanning angle is less than 80° and the
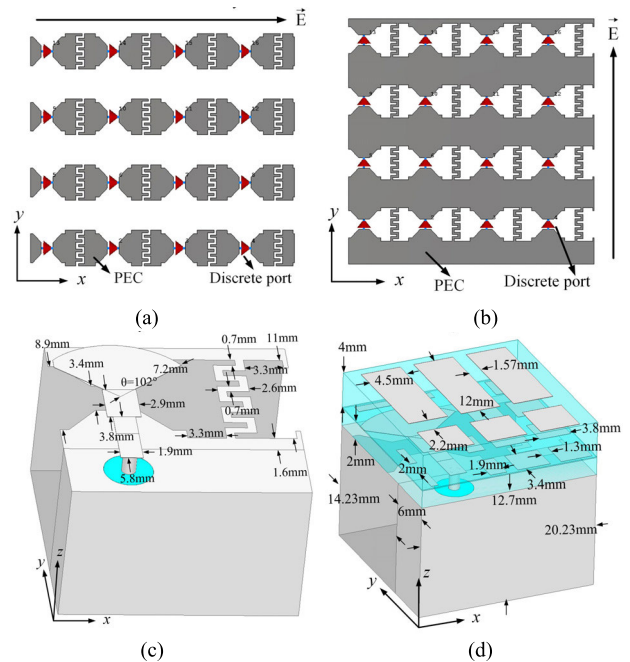

FIGURE 1. (a) A 4 × 4 TCDA without the feeding network and the WAIM layer. (b) A 4 × 4 SC-TCDA without the feeding network and the WAIM layer. (c) The SC-TCDA element with the feeding network but without the WAIM layer. (d) The SC-TCDA element with the feeding network and the WAIM layer.

bandwidth is less than 2:1. According to the proposed TCDA structure and wide-angle matching layer, an array with ±80° scanning in the E plane in 2.2-5.95 GHz is proposed, which is shown in Figs. 1(c) and (d). The SC-TCDA element with the feeding network but without the WAIM layer is shown in Fig. 1(c). The bottom structure of the SC-TCDA is the metal reflecting cavity. If the metal cavity is changed to a planar reflector, the VSWRs will change a little. But, the patterns will get worse. The feed part of the SC-TCDA is a sector structure, and the coaxial line passes through the side metal wall. The SC-TCDA element with the feeding network and the WAIM layer is shown in Fig. 1(d). The WAIM layer at the upper surface of the SC-TCDA can improve the scanning angle [13]. The WAIM layer has only one-layer PCB, which is composed of the upper and lower metal layers. The proposed SC-TCDA has only two layers of dielectric substrates. The final size of the antenna element is 20.2 mm × 20.2 mm × 18.8 mm.

Figs. 2(a) and (b) are the equivalent models of Figs. 1(a) and (b), respectively. C in Fig. 2(a) is the series capacitance of the TCDA, and L in Fig. 2(b) is the parallel inductance of the SC-TCDA.

To relate the impedance values of the two complimentary surfaces, the Babinet's principle is used, which is (from Chapter 6 in [15])

$$Z_W Z_S = Z_{\mathrm{m}}^2/4 \qquad (1)$$

where Z_w is the impedance of the TCDA, Z_s is the impedance of the SC-TCDA, and Z_m is the intrinsic impedance of the medium (for free space, $Z_m = 377\ \Omega$).
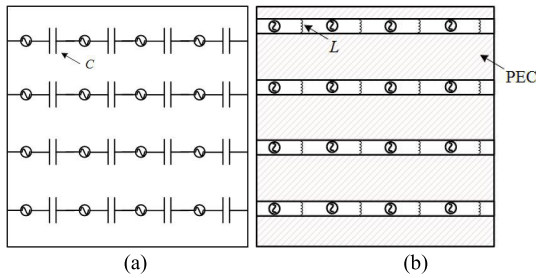
FIGURE 2. (a) An equivalent model of Fig. 1(a). (b) An equivalent model of Fig. 1(b).
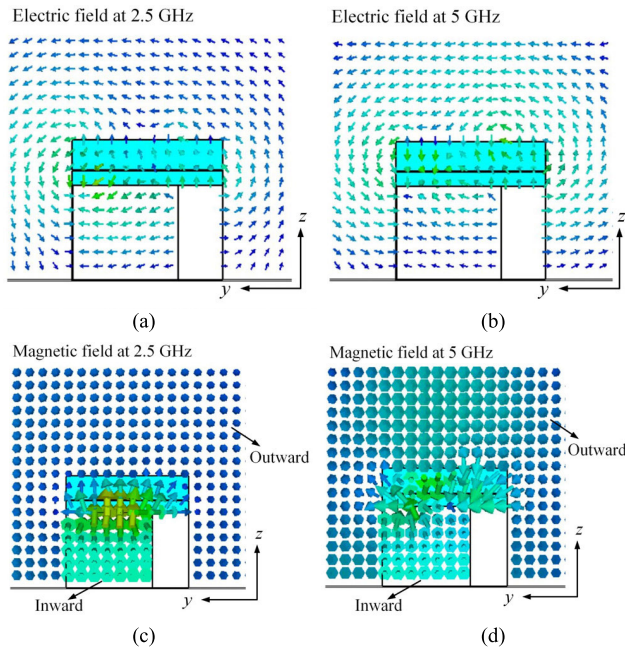

FIGURE 3. The electric field and magnetic field distributions of a 1 ×∞ array of the SC-TCDA of Fig. 1(d) in the *x* direction. (a) The electric field distributions at 2.5 GHz. (b) The electric field distributions at 5 GHz. (c) The magnetic field distributions at 2.5 GHz. (d) The magnetic field distributions at 5 GHz.

From Babinet's principle, the relationship between the capacitance (*C*) and the inductance (*L*) is

$$Z_W Z_S = \left(\frac{1}{j\omega C}\right)(j\omega L) = \frac{L}{C} = Z_{\mathrm{m}}^2/4 \qquad (2)$$

B. EQUIVALENT MAGNETIC CURRENT CHARACTERISTICS

In order to analyze the equivalent magnetic current characteristics of the SC-TCDA shown in Fig. 1(d), the electric field and magnetic field are simulated by CST, which are shown in Fig. 3. The simulated model in Fig. 3 is a 1 ×∞ array of the SC-TCDA of Fig. 1(d) in the *x* direction, which has an infinite PEC ground plane. Figs. 3(a) and (c) are the electric field and the magnetic field distributions of the SC-TCDA at 2.5 GHz, respectively. Figs. 3(b) and (d) are the electric field and the magnetic field distributions of the SC-TCDA at 5 GHz, respectively. In Figs. 3(a) and (b), the directions of the electric fields on the right side are upward, the directions of the electric fields on the upper side are leftward, and the directions of the electric fields on the left side are downward.
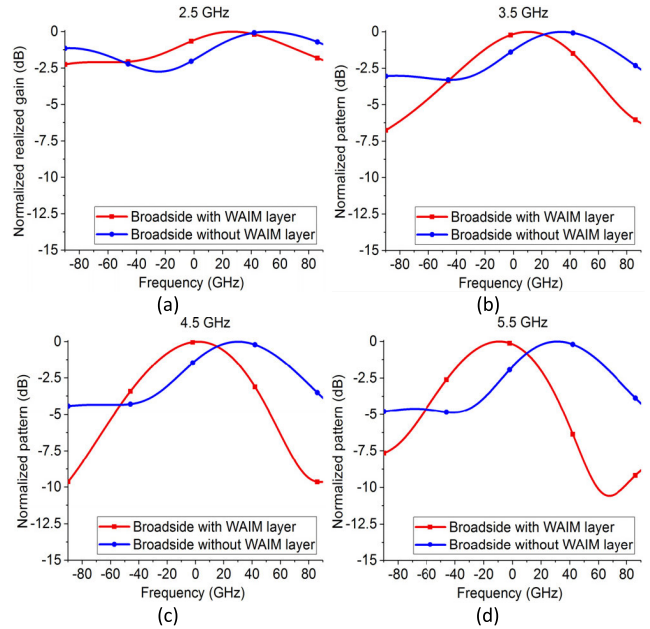

FIGURE 4. The comparison of the detailed patterns of the antenna element with and without a WAIM layer.

However, the directions of the electric fields inside the metal cavity are opposite to the directions of the external electric fields. The magnetic field distributions of the SC-TCDA of Fig. 1(d) are shown in Figs. 3(c) and (d). It can be seen that the directions of the magnetic fields inside the metal cavity are inward. However, the directions of the magnetic fields outside the metal cavity are outward. So the directions of magnetic fields are opposite inside and outside the metal cavity.

Based on the above analysis, the electric field and magnetic field distributions above the slot can be equivalent to the outward magnetic current, and the electric field and magnetic field distributions under the slot can be equivalent to the inward magnetic current. Therefore, the SC-TCDA can be equivalent to two magnetic currents above and below the slot PEC plane. The above conclusions are consistent with those in Ref. [4]. Since the equivalent magnetic current under the slot is surrounded by the metal cavity, the electric fields and magnetic fields in the cavity cannot be radiated to the outside. Therefore, the SC-TCDA can be equivalent to a magnetic current above the slot.

The patterns of the SC-TCDA element in Fig. 1(d) for an infinite array at 2.5 GHz, 3.5 GHz, 4.5 GHz, and 5.5 GHz in the E plane are shown in Fig. 4. The E plane of the SC-TCDA is the *yz* plane in Fig. 1(d). It can be seen that the 3dB beamwidth in the E plane at different frequencies are very wide. Especially at 2.5 GHz, the 3dB beamwidth in the E plane can reach 180°. Therefore, the 3dB beamwidths of the SC-TCDA in the E plane are close to that of the ideal magnetic current, which is parallel to the infinite ground plane. The 3-dB beamwidths at high frequencies are not very good, which is mainly due to the influence of the WAIM layer. If the antenna element is without a WAIM layer, the 3-dB beamwidth can reach 180° at low frequencies and the
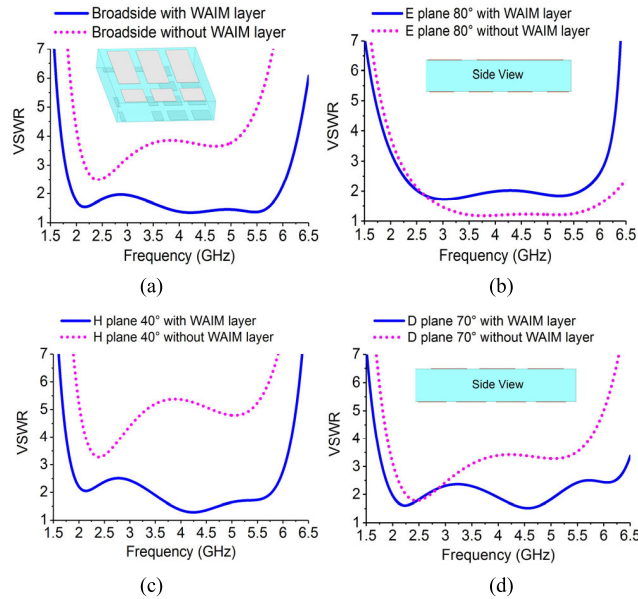
FIGURE 5. The VSWRs with and without the WAIM layer. (a) At the broadside. (b) 80° scanning in the E plane. (c) 40° scanning in the H plane. (d) 70° scanning in the D plane.

5-dB beamwidth also can reach 180° at high frequencies. The comparison of the detailed patterns of the antenna element with and without a WAIM layer is shown in Fig. 4. Moreover, the wide beamwidth of the SC-TCDA in the E plane is very helpful for the wide-angle scanning in the E plane.

C. WAIM LAYER ANALYSIS

Because the input impedances will change greatly when scanning at a large angle, it is necessary to add a WAIM layer to get a better impedance matching and increase the scanning angle [13]. Then, a single-layer WAIM layer with bilateral metal layers is added to the SC-TCDA, which is shown in Fig. 5(a). The VSWRs of the SC-TCDA with and without the WAIM layer at different scanning angles are compared in Fig. 5. At the broadside, the maximum VSWR without the WAIM layer is changed from 2 to 7 in 2.2-5.95 GHz in Fig. 5(a). In Fig. 5(b), we can find that the VSWR of the SC-TCDA without the WAIM layer at 80° in the E plane is much better than that of the SC-TCDA without the WAIM layer at the broadside. This is mainly due to the variation of radiation impedance when scanning in the E plane [16], [17]. In the H plane, the maximum VSWR without the WAIM layer is changed from 2.5 to 7 in 2.2-5.95 GHz in Fig. 5(c). In the D plane, the maximum VSWR without the WAIM layer is changed from 2.5 to 5 in 2.2-5.95 GHz in Fig. 5(d). We can see that the VSWRs become better when the SC-TCDA is loaded with the WAIM layer in 2.2-5.95 GHz in different planes. Therefore, the WAIM layer can increase the scanning bandwidth of the SC-TCDA.

III. SIMULATED AND MEASURED RESULTS
A. SIMULATED ANTENNA EFFICIENCIES

The simulated antenna efficiencies in different planes for an infinite array are shown Fig. 6. The two PCB layers of the SC-TCDA are the F4B, which have a relative permittivity
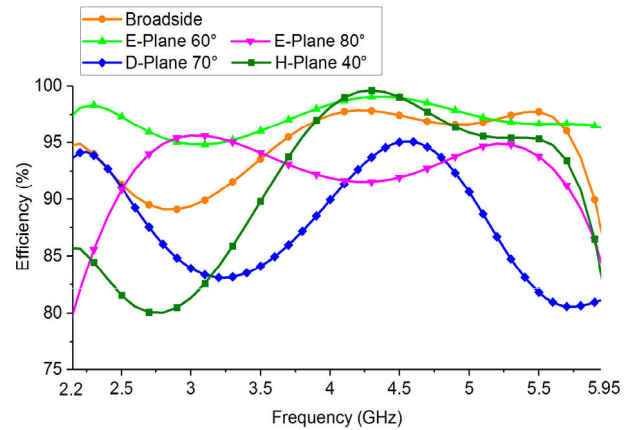

FIGURE 6. Simulated efficiencies in different planes for an infinite array.

of 2.2 and a dielectric loss tangent of 0.003 with very low losses. We can see that the efficiencies exceed 80% in 2.2-5.95 GHz. Therefore, the proposed SC-TCDA has high efficiencies in different planes.

B. SIMULATED ACTIVE VSWRs

In Figs. 7(a), (b), and (c), the simulated active VSWRs of the proposed SC-TCDA for an infinite array are shown. The scanning range is from −88° to 88° in 1.5-6.5 GHz. In order to clearly see the scanning characteristics, the curves of VSWRs of 2, 2.5, and 3 are marked in Fig. 7.

At broadside, we can see that the VSWRs are less than 2.5 in 1.85-6.05 GHz. In the E plane, the VSWRs are less than 2.5 in 2.2-5.95 GHz when the scanning range is from −80° to 80°. In the H plane, the VSWRs are less than 2.5 when the scanning range is from −40° to 40° in 1.9-6 GHz. In the D plane, the VSWRs are less than 2.5 in 1.85-6.15 GHz when the scanning range is from −70° to 70°. When the active VSWRs are less than 2.5, the maximum scanning angles of the proposed SC-TCDA are ±80°, ±40°, and ±70° in Figs. 7(a), (b), and (c), respectively. And there is no scanning blindness in the E, H, and D planes. Although the phased array in [9] can achieve 50° scanning in the H plane, there are 11 dielectric substrate layers above the array. In [8], the phased array can achieve 50° scanning in the H plane, but 13 dielectric substrate layers are loaded above the array. It can be seen that they used many layers of dielectric blocks to increase the scanning angle in the H plane. So, it is hard to match the impedance in the H plane in [6]–[9]. However, in this paper, only a dielectric substrate layer of the WAIM layer is loaded, which can reduce the design complexity of the WAIM layer and achieve ±80° scanning in the E plane. Therefore, the proposed SC-TCDA has a wide-band impedance matching and wide-angle scanning characteristics.

C. MEASURED RESULTS

To verify the proposed SC-TCDA, an array shown in Fig. 8(a) is fabricated, which has 16 × 16 elements. The experimental setup includes coaxial lines, power dividers, time delay lines, and an antenna turntable, which are shown
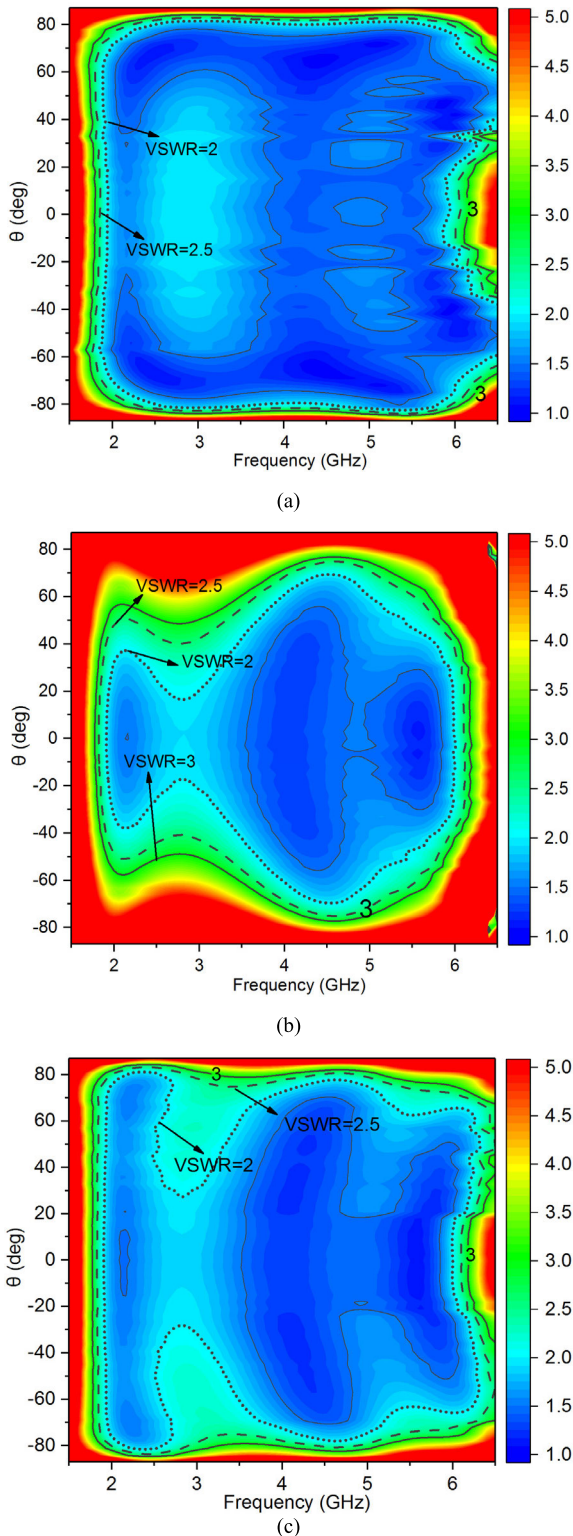
(a)

(b)

(c)

FIGURE 7. (a) The simulated active VSWRs in the E plane. (b) The simulated active VSWRs in the H plane. (c) The simulated active VSWRs in the D plane.

in Fig. 8(b). The size of the proposed SC-TCDA is 324 mm × 324 mm × 18.8 mm. A group of time delay lines are needed to be changed when another scanning angle of the array is measured.

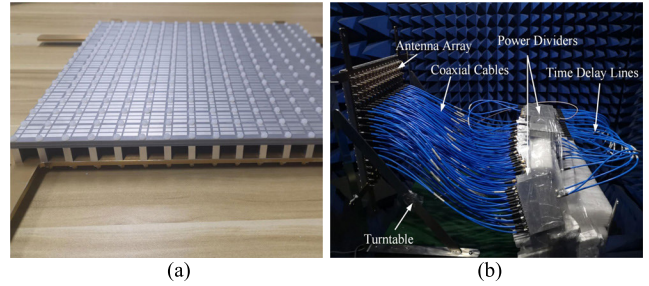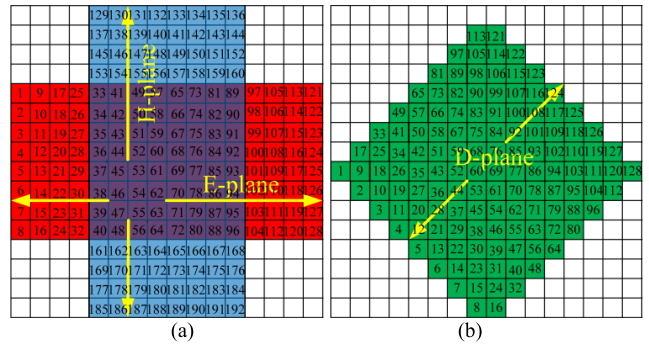**FIGURE 8.** (a) The proposed array. (b) The measured environment.

(a)

(b)

FIGURE 9. The measured plan. (a) E and H planes. (b) D plane.

The measured elements in a 16 × 16 array are marked with red, blue, and green colors in Fig. 9. Because there are only 19 8-in-1 combiners with the same amplitudes and phases, only the 8 × N ports of the array can be measured. The measured 8 × 16 elements with red color and blue color in the E and H planes are shown in Fig. 9(a), respectively. The measured 8 × 16 elements with green color in the D plane are shown in Fig. 9(b). When the arrays with 8 × N ports are measured, the other antenna elements with white colors are loaded with 50 Ω matching loads.

The details on how the array is measured with the time delay lines are as follows. Firstly, according to the scanning angle, such as broadside, ±60° in the E plane, ±80° in the E plane, ±40° in the H plane, ±60° in the D plane, and ±70° in the D plane, corresponding six groups of different coaxial delay lines should be prepared. Each group of time delay lines has 16 coaxial lines with different time delays. If the 80° in the E plane is measured, the E plane of the array needs to be parallel to the ground. Then, antenna elements 1-8 in Fig. 9(a) are connected with an 8-in-1 combiner by 8 coaxial lines of the same amplitudes and phases. Then the output of the 8-in-1 combiner is connected with the first time delay coaxial line. Similarly, antenna elements 121-128 in Fig. 9(a) are connected with another 8-in-1 combiner by 8 coaxial lines of the same amplitude and phase. And the output of the 8-in-1 combiner is connected with the sixteenth time delay coaxial line. If the 40° in the H plane is measured, Fig. 9(a) needs to be rotated 90° to the right. Then, antenna elements 185-192 in Fig. 9(a) are connected with an 8-in-1 combiner. Similarly, antenna elements 129-136 in Fig. 9(a) are connected with another 8-in-1 combiner. If the 70° in the D plane is measured, Fig. 9(a) needs to be rotated 45° to
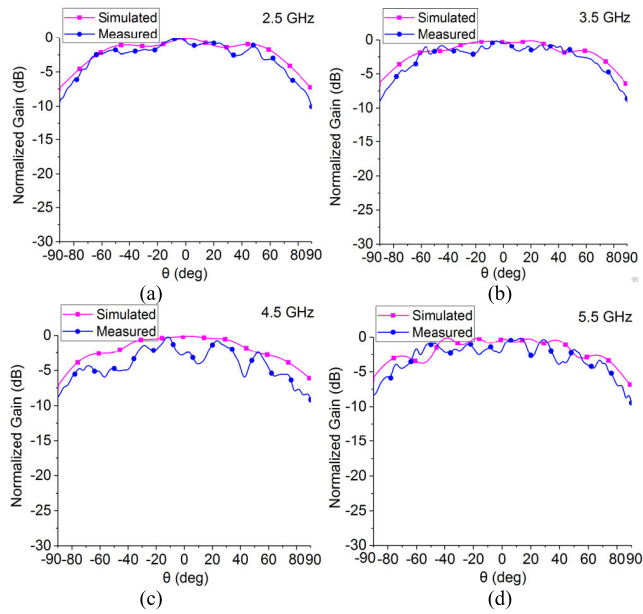
FIGURE 10. The patterns of the middle antenna element at different frequencies in the E plane.
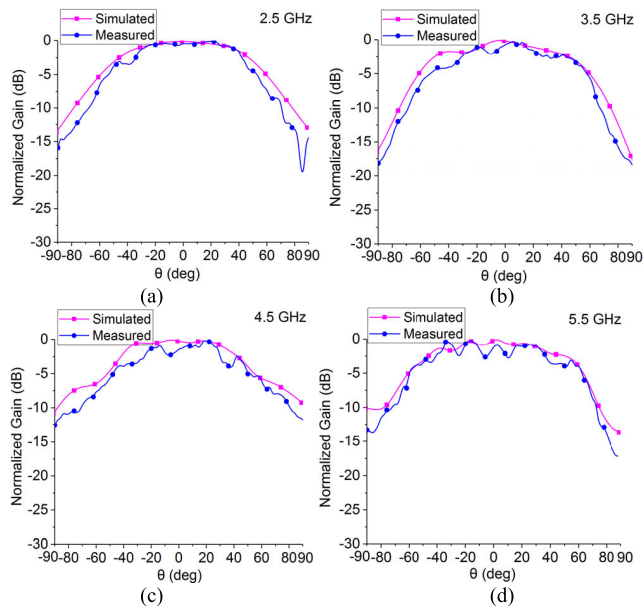

FIGURE 11. The patterns of the middle antenna element at different frequencies in the H plane.

FIGURE 12. The simulated and measured normalized patterns in the E plane at 0°, ±60°, and ±80° scanning.
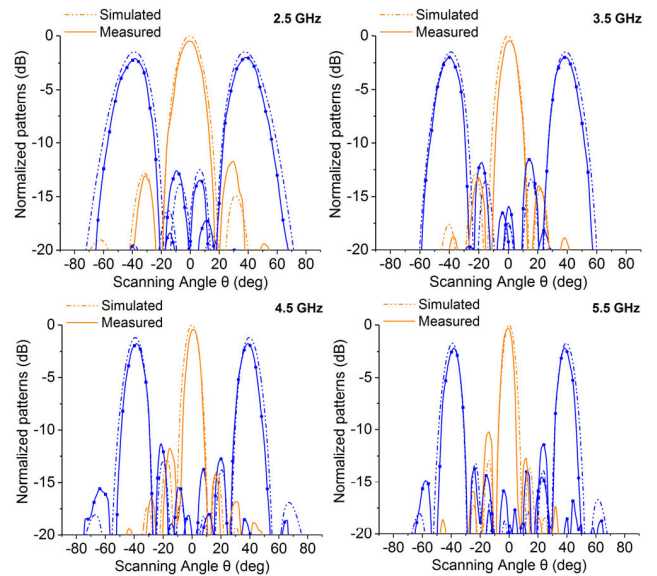
FIGURE 13. The simulated and measured normalized patterns in the H plane at 0° and ±40°.

the right. And the E plane of the array is 45° to the ground plane. Then, antenna elements 1-8 in Fig. 9(b) are connected with an 8-in-1 combiner. Similarly, antenna elements 121-128 in Fig. 9(b) are connected with another 8-in-1 combiner. When other scanning angles are measured, only 16 coaxial time delay lines need to be replaced.

The patterns of the middle element in the 16×16 array are simulated and measured in the E and H planes when other elements are loaded with 50 Ω matching loads. The patterns at 2.5 GHz, 3.5 GHz, 4.5 GHz, and 5.5 GHz in the E and H planes are shown in Fig. 10 and Fig. 11, respectively. As shown in Fig. 10, the patterns of the middle element in the E plane at different frequencies have a wide 3dB beamwidth.
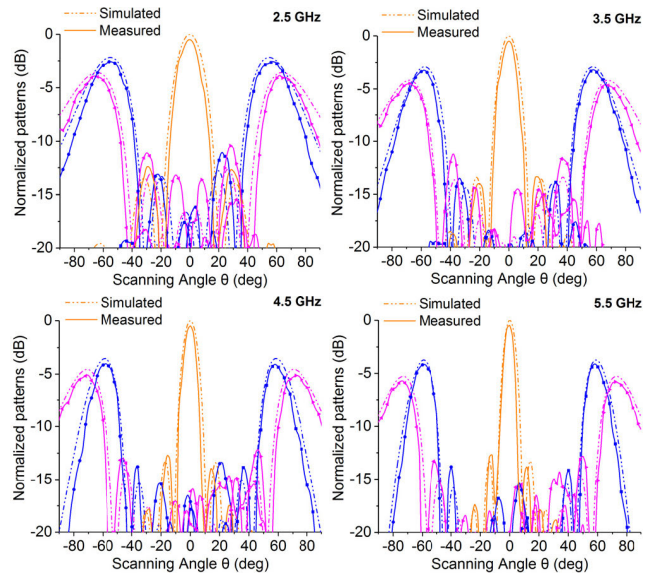
In Fig. 11, the patterns of the middle element in the H plane have a narrow 3dB beamwidth, because the pattern of the slot antenna is identical in shape to that of the dipole antenna except that the E- and H-fields are interchanged [18]. The wider the 3dB beamwith of the antenna element, the larger the scanning angle. We can see that the SC-TCDA has a wide-band and wide-angle scanning characteristics in the E plane.

Figs. 12, 13, and 14 are the patterns of the proposed SC-TCDA in different planes. The gains in Figs. 12-14 are divided by the maximum simulated gain at the broadside. In the E plane, the patterns of the proposed SC-TCDA at the scanning angles of 0°, ±60°, and ±80° are measured. As shown in Fig. 12, when the array is scanned at 80° in the

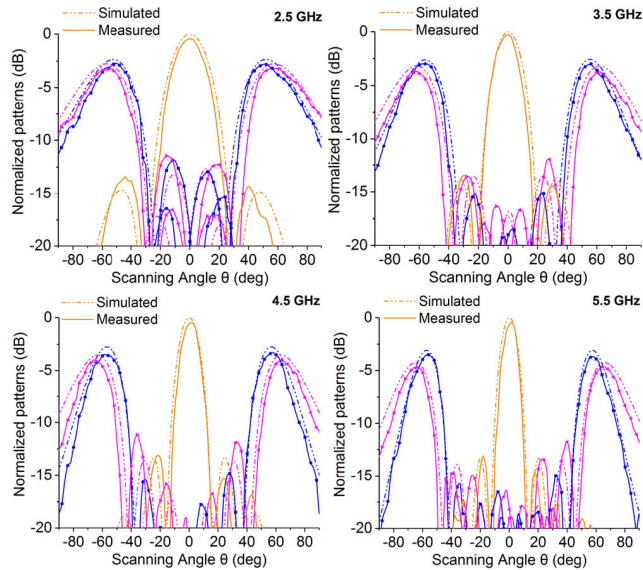**FIGURE 14.** The simulated and measured normalized patterns in the D plane at 0°, ±60°, and ±70°.

E plane, the directions of the main beams can reach 65° and 74° at 2.5 GHz and 5.5 GHz, respectively. In the H plane, the patterns of the array at the scanning angles of 0° and ±40° are measured. We can see that the directions of the main beams can point at 40° in Fig. 13. In the D plane, the patterns of the array at the scanning angles of 0°, ±60°, and ±70° are measured. As shown in Fig. 14, when the array is scanned at 70° in the D plane, the directions of the main beams can reach 57° and 66° at 2.5 GHz and 5.5 GHz, respectively.

We can see that the maximum scanning angles of the proposed array can reach 74°, 40°, and 66° when scanning to 80°, 40°, and 70° at 5.5 GHz in the E, H, and D planes, respectively. But at 2.5 GHz, the maximum scanning angles of the proposed array only can reach 65° and 57° when scanning to 80° and 70° in the E and D planes, respectively. The reason is that the maximum scanning angle is affected by the pattern of antenna element and array factor. The main beams of the isotropic point source array with any element distances at different frequencies can be accurately pointed to the scanning angles. When the distance between the point source antennas becomes smaller, the beam width of the array factor will be wider. Therefore, the maximum scanning angle is affected by the pattern of antenna element and the size of the array. If the size of the array is 64 × 64, the beam direction of the array at 2.5 GHz will close to the scanning angle. The patterns of a 32 × 32 array and a 64 × 64 array at 2.5 GHz and 5.5 GHz are shown in Fig. 15 when scanning to 80° in the E plane. Therefore, as the size of the array increases, the directions of the main beams at 2.5 GHz and 5.5 GHz are closer to 80°.

The measured maximum realized gains at different angles are shown in Fig. 16. The blue solid line is the ideal aperture gain of the 8 × 16 array at the broadside. The blue gain curve with short dots represents the measured realized gain of the 8 × 16 array at the broadside. The gain curve with
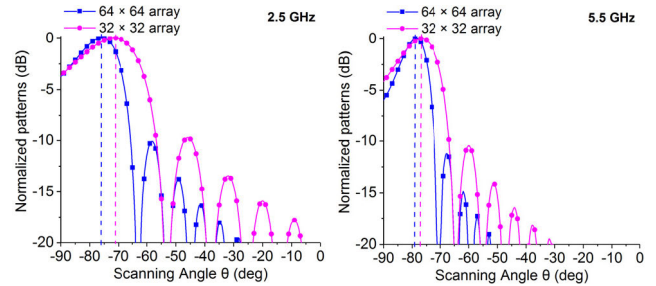

FIGURE 15. Normalized patterns of a 32 × 32 array and a 64 × 64 array in the E plane when scanning at 80° at different frequencies.
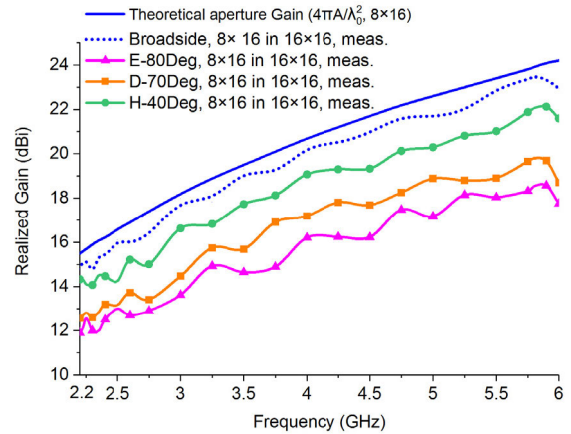
FIGURE 16. The co-polarization and cross-polarization of the proposed array.
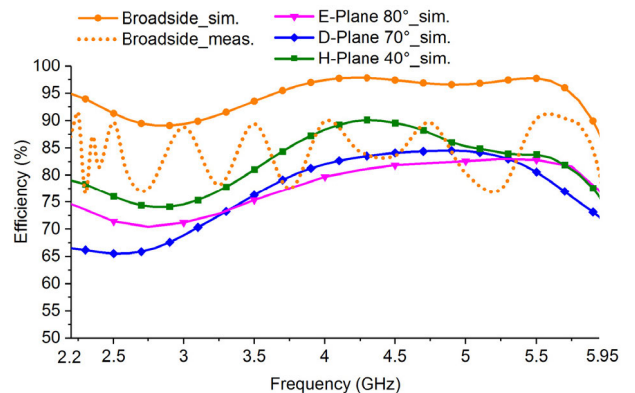
FIGURE 17. The simulated and measured radiation efficiencies of a 16 × 8 array at different scanning angles.

triangle marks represents the measured realized gain of the 8 × 16 array when scanning at 80° in the E plane. The gain curve with dot marks represents the measured realized gain of the 8 × 16 array when scanning at 40° in the H plane. The gain curve with square marks represents the measured gain of the 8 × 16 array when scanning at 70° in the D plane. The figure shows that the gains of the array gradually increase with frequencies and decrease with scanning angles.

The simulated and measured radiation efficiencies of a 16 × 8 array at different scanning angles are shown in Fig. 17. The simulated radiation efficiencies at different

FIGURE 18. Normalized cross polarizations at different scanning angles.

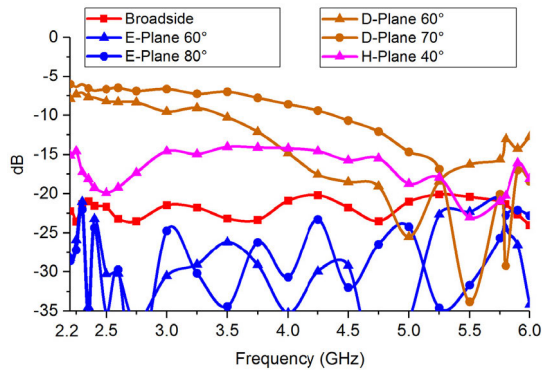**TABLE 1.** Comparison between the proposed work and other works.

Ref.	BW	E-θ_{max}	H-θ_{max}	D-θ_{max}	LW (λ_{high})	THK (λ_{low})	WAIM layers	VSWR	POL
[8]	2.2:1	50°	50°	50°	0.46	0.2	13	2	Single
[9]	5:1	50°	50°	50°	0.45	0.15	11	2.5	Dual
[21]	5.4:1	45°	45°	45°	0.4	0.1	1	3.1	Single
This work	2.7:1	80°	40°	70°	0.4	0.138	1	2.5	Single

scanning angles are marked with solid lines. The measured radiation efficiencies at the broadside are marked with short dot lines. The measured radiation efficiencies at the broadside are obtained by dividing the measured gain by the aperture directivity, which is more than 75%. We can see that the simulated efficiencies are more than 65% in the band of 2.2-5.95 GHz at different scanning angles. Therefore, the proposed SC-TCDA has high efficiencies in different planes.

The measured normalized cross polarizations at different scanning angles in different planes are shown in Fig. 18. The cross polarization level is based on the Ludwig's third definition [19]. It can be seen that the normalized cross polarizations are below −20 dB when scanning at 0°, 60°, and 80° in the E plane. The normalized cross polarizations are less than −14 dB at the scanning angle of 40° in the H plane. The cross polarizations are poor at the scanning angles of 60° and 70° in the D plane. The cross-polarizations of the theoretical values at the scanning angles of 60° and 70° in the D plane are 9.5 dB and 6 dB, respectively [20]. Because the SC-TCDA is the single- polarization array, the cross polarizations of the SC-TCDA in the D plane are close to the theoretical values at different scanning angles.

Table 1 shows the comparison between the proposed work and other relevant works. In Table 1, LW, THK and POL represent the length and width of the antenna element, the thickness of the array and the polarization of the array, respectively. We can see that the proposed SC-TCDA has a wide-band, a wide-scanning angle, a low profile, and one WAIM layer. The proposed array can work over the band of 2.2-5.95 GHz (VSWRs<2.5) and can scan to ±80° in the E plane. According to the results, this proposed array is very attractive.

IV. CONCLUSION

In order to achieve a larger scanning angle, an antenna unit with a wide 3dB beamwidth is needed. Because the electric current antenna has a narrow 3dB beamwidth in the E plane, it is difficult to achieve a large scanning angle in the E plane. But the magnetic current antenna has a wide 3dB beamwidth, which is close to 180° in the E plane. Therefore, the magnetic current array is helpful to achieve a large scanning angle in the E plane. In this paper, a novel broadband self-complementary tightly-coupled dipole array is proposed to achieve a wide-band and wide-angle magnetic current antenna, which can scan to ±80° in the E plane. The antenna structure, the equivalent magnetic current characteristics and the WAIM layer are analyzed. The electric field and the magnetic field distributions of the SC-TCDA are also analyzed. The 3dB beamwidths of the SC-TCDA are close to 180° in the E plane in a wide band. When the VSWRs are less than 2.5, the SC-TCDA can scan to ±80°, ±40°, and ±70° in the E, H, and D planes, respectively. At last, an SC-TCDA with 16 × 16 elements is fabricated and measured. The measured and simulated results are in good agreement. Therefore, a wide-band and wide-angle phased array is achieved by using the SC-TCDA.

REFERENCES

[1] R. Wang, B.-Z. Wang, X. Ding, and X.-S. Yang, "Planar phased array with wide-angle scanning performance based on image theory," *IEEE Trans. Antennas Propag.*, vol. 63, no. 9, pp. 3908–3917, Sep. 2015.

[2] J. Liu and Q. Xue, "Microstrip magnetic dipole Yagi array antenna with endfire radiation and vertical polarization," *IEEE Trans. Antennas Propag.*, vol. 61, no. 3, pp. 1140–1147, Mar. 2013.

[3] R. Wang, B.-Z. Wang, C. Hu, and X. Ding, "Wide-angle scanning planar array with quasi-hemispherical-pattern elements," *Sci. Rep.*, vol. 7, no. 1, p. 2729, Jun. 2017.

[4] A. Neto and J. J. Lee, "'Infinite bandwidth' long slot array antenna," *IEEE Antennas Wireless Propag. Lett.*, vol. 4, pp. 75–78, Jan. 2005.

[5] A. Neto and J. J. Lee, "Ultrawide-band properties of long slot arrays," *IEEE Trans. Antennas Propag.*, vol. 54, no. 2, pp. 534–543, Feb. 2006.

[6] J. F. McCann, R. J. Marhefka, and B. A. Munk, "An array of slot elements for wide scan angles and large bandwidth," in *Proc. IEEE Antennas Propag. Soc. Int. Symp.*, Albuquerque, NM, USA, Jul. 2006, pp. 3027–3030.

[7] O. Yurduseven, D. Cavallo, and A. Neto, "Wideband dielectric lens antenna with stable radiation patterns fed by coherent array of connected leaky slots," *IEEE Trans. Antennas Propag.*, vol. 62, no. 4, pp. 1895–1902, Apr. 2014.

[8] W. H. Syed, D. Cavallo, H. T. Shivamurthy, and A. Neto, "Wideband, wide-scan planar array of connected slots loaded with artificial dielectric superstrates," *IEEE Trans. Antennas Propag.*, vol. 64, no. 2, pp. 543–553, Feb. 2016.

[9] D. Cavallo, W. H. Syed, and A. Neto, "A 5:1 connected slot array loaded with artificial dielectric layers," in *Proc. IEEE Int. Symp. Phased Array Syst. Technol. (PAST)*, Waltham, MA, USA, Oct. 2016, pp. 1–4.

[10] B. Munk, R. Taylor, T. Durharn, W. Croswell, B. Pigon, R. Boozer, S. Brown, M. Jones, J. Pryor, S. Ortiz, J. Rawnick, K. Krebs, M. Vanstrum, G. Gothard, and D. Weibelt, "A low-profile broadband phased array antenna," in *Proc. IEEE Antennas Propag. Soc. Int. Symp.*, Columbus, OH, USA, vol. 2, Jun. 2003, pp. 448–451.

[11] B. A. Munk, "Broadband wire arrays," in *Finite Antenna Arrays and FSS*, 1st ed. Hoboken, NJ, USA: Wiley-IEEE Press, 2003, ch. 6, pp. 181–213.

[12] M. Jones and J. Rawnick, "A new approach to broadband array design using tightly coupled elements," in *Proc. MILCOM-IEEE Mil. Commun. Conf.*, Orlando, FL, USA, Oct. 2007, pp. 1–7, doi: 10.1109/MILCOM.2007.4454764.

[13] E. Magill and H. Wheeler, "Wide-angle impedance matching of a planar array antenna by a dielectric sheet," *IEEE Trans. Antennas Propag.*, vol. 14, no. 1, pp. 49–53, Jan. 1966.

[14] Y. Mushiake, "Self-complementary antennas," *IEEE Antennas Propag. Mag.*, vol. 34, no. 6, pp. 23–29, Dec. 1992.

[15] B. A. Munk, *Frequency Selective Surfaces: Theory and Design*. New York, NY, USA: Wiley, 2000.

[16] H. Wheeler, "Simple relations derived fom a phased-array antenna made of an infinite current sheet," *IEEE Trans. Antennas Propag.*, vol. AP-13, no. 4, pp. 506–514, Jul. 1965.

[17] H. A. Wheeler, "The radiation resistance of an antenna in an infinite array or waveguide," *Proc. IRE*, vol. 36, no. 4, pp. 478–487, Apr. 1948.

[18] C. A. Balanis, *Antenna Theory: Analysis and Design*, 3rd ed. Hoboken, NJ, USA: Wiley, 2005.

[19] A. Ludwig, "The definition of cross polarization," *IEEE Trans. Antennas Propag.*, vol. AP-21, no. 1, pp. 116–119, Jan. 1973.

[20] J. A. Kasemodel, C.-C. Chen, and J. L. Volakis, "Wideband planar array with integrated feed and matching network for wide-angle scanning," *IEEE Trans. Antennas Propag.*, vol. 61, no. 9, pp. 4528–4537, Sep. 2013.

[21] H. Zhang, S. Yang, Y. Ou, and Y. Chen, "Low cross-polarization ultrawideband planar antenna array," in *Proc. IEEE Int. Symp. Antennas Propag. USNC/URSI Nat. Radio Sci. Meeting*, San Diego, CA, USA, Jul. 2017, pp. 1327–1328.

CHANGHAI HU was born in Chongqing, China, in 1987. He received the B.S. and M.S. degrees in computer science and technology and electromagnetic field and microwave technology from Southwest Jiaotong University (SWJTU), Chengdu, China, in 2010 and 2014, respectively. He is currently pursuing the Ph.D. degree in radio physics with the University of Electronic Science and Technology of China (UESTC), Chengdu. His main research interests include ultra-wideband and wide-angle scanning phased array antennas.

BING-ZHONG WANG (Senior Member, IEEE) received the Ph.D. degree in electronic engineering from the University of Electronic Science and Technology of China (UESTC), Chengdu, in 1988.

He joined UESTC, in 1984, where he is currently a Professor. He has been a Visiting Scholar with the University of Wisconsin–Milwaukee, Milwaukee, WI, USA, a Research Fellow with the City University of Hong Kong, Hong Kong, and a Visiting Professor with the Electromagnetic Communication Laboratory, Pennsylvania State University, University Park, PA, USA. His current research interests include computational electromagnetics, antenna theory and techniques, and time-reversed electromagnetics.

BIN FENG SUN was born in Shanxi, China, in 1995. He received the B.S. degree in electronic information science and technology from Shanxi University (SXU), Shanxi, in 2017. He is currently pursuing the M.S. degree in radio physics with the University of Electronic Science and Technology of China (UESTC), Chengdu, China. His main research interests include wide-angle scanning array and optimization algorithm.

REN WANG (Member, IEEE) was born in Anhui, China, in 1990. He received the B.S. and Ph.D. degrees in electronic information science and technology and radio physics from the University of Electronic Science and Technology of China (UESTC), Chengdu, in 2014 and 2018, respectively. He worked at the Optoelectronics Research Centre, University of Southampton, U.K., as a Visiting Scholar, from September 2016 to September 2017. He is currently a Research Fellow with UESTC. His main research interests include phased arrays, metasurfaces, and time-reversed electromagnetics.

SHAOQIU XIAO (Member, IEEE) was born in September 1975. He received the Ph.D. degree in electro-magnetic field and microwave technology from the University of Electronic Science and Technology of China (UESTC), Chengdu, China, in 2003. From January 2004 to June 2004, he joined UESTC as an Assistant Professor. From July 2004 to March 2006, he worked for the Wireless Communications Laboratory, National Institute of Information and Communications Technology of Japan (NICT), Singapore, as a Research Fellow with the focus on the planar antenna and smart antenna design and optimization. From July 2006 to June 2010, he worked for UESTC as an Associate Professor. He visited the Ecole Normale Superieure de Cachan, Paris, France, as a Senior Research Scholar, from July 2015 to August 2015. He is currently working for UESTC as a Professor. He has authored/coauthored more than 240 technical journals, conference papers, books and book chapters. His current research interests include planar antenna and phased array, computational electromagnetics, microwave passive circuits, and time reversal electromagnetics.

SAN-QIANG TONG (Graduate Student Member, IEEE) received the B.S. and M.S. degrees from the University of Electronic Science and Technology of China (UESTC), Chengdu, China, in 2011 and 2016, respectively, where he is currently pursuing the Ph.D. degree in radio physics. His main research interests include wide-band and wide-angle scanning phased arrays, low profile antenna arrays, and miniaturized antenna arrays.

XIAO DING (Member, IEEE) received the Ph.D. degree in radio physics from the University of Electronic Science and Technology of China (UESTC), Chengdu, China, in 2014.

He joined UESTC, in 2014. In 2013, he was a Visiting Scholar with the Department of Electrical and Computer Engineering, South Dakota School of Mines and Technology, Rapid City, SD, USA. From June 2016 to June 2017, he was a Visiting Scholar with the Applied Electromagnetics Laboratory, University of Houston, Houston, TX, USA. He is currently an Associate Professor with UESTC. His research interests include antenna theory and computational electromagnetics.

● ● ●